nature structural & molecular biology

EttA regulates translation by binding the ribosomal E site and restricting ribosome-tRNA dynamics

Bo Chen[1], Grégory Boël[1,2,6], Yaser Hashem[3,6], Wei Ning[4], Jingyi Fei[4,5], Chi Wang[1], Ruben L Gonzalez Jr[4], John F Hunt[1,2] & Joachim Frank[1,3]

Cells express many ribosome-interacting factors whose functions and molecular mechanisms remain unknown. Here, we elucidate the mechanism of a newly characterized regulatory translation factor, energy-dependent translational throttle A (EttA), which is an *Escherichia coli* representative of the ATP-binding cassette F (ABC-F) protein family. Using cryo-EM, we demonstrate that the ATP-bound form of EttA binds to the ribosomal tRNA-exit site, where it forms bridging interactions between the ribosomal L1 stalk and the tRNA bound in the peptidyl-tRNA–binding site. Using single-molecule fluorescence resonance energy transfer, we show that the ATP-bound form of EttA restricts ribosome and tRNA dynamics required for protein synthesis. This work represents the first example, to our knowledge, in which the detailed molecular mechanism of any ABC-F family protein has been determined and establishes a framework for elucidating the mechanisms of other regulatory translation factors.

The efficient function of cells requires that ribosome biogenesis and activity be regulated in response to changing environmental and metabolic conditions[1]. However, the understanding of the molecular mechanisms of many of these regulatory processes has remained limited, despite their biological importance. Many ribosome-interacting proteins beyond the canonical translation factors have been identified that are believed to function as regulatory translation factors[1,2]. Unfortunately, it has been possible to elucidate the exact physiological role and mechanism of action for only a relatively small subset of such regulatory translation factors. The limited progress in this area has impeded the development of atomic-resolution mechanistic models for translation regulation, despite the tremendous progress that has been made over the past two decades in understanding ribosome structure[2,3] and many other aspects of protein synthesis. In the current study, we used a combination of biophysical methods to develop such a model for a new translational regulatory factor called EttA, which, to our knowledge, is characterized for the first time in Boël *et al.*[4]. Close coordination of the work reported in these two papers has provided a unique opportunity to dissect the function and mechanism of EttA, which belongs to the ubiquitously distributed but minimally characterized ABC-F protein family.

Protein synthesis by the ribosome is a highly dynamic molecular process, particularly during the stage of polypeptide chain elongation. This stage involves cyclical execution of three steps[2]: (i) binding of a cognate aminoacylated tRNA to the mRNA codon at the aminoacyl-tRNA–binding (A) site on the ribosome; (ii) synthesis of the next peptide bond in the peptidyl transferase center (PTC) on the ribosome, a process that results in transfer of the nascent polypeptide chain from the tRNA bound in the peptidyl-tRNA–binding (P) site to the newly bound tRNA in the A site; and (iii) translocation of the mRNA and the cognate tRNAs located in both the P and A sites, which moves these tRNAs to the exit (E) and P sites, respectively. Cryo-EM[5,6] and single-molecule fluorescence resonance energy transfer (smFRET)[7–11] measurements have been used to characterize the structure and dynamics of the ribosomal pretranslocation (PRE) complex that has completed the first two steps in the elongation cycle but not the third. These studies demonstrate that the PRE complex exists in a spontaneous equilibrium between two global conformational states, called macrostates I and II (MS-I and MS-II)[12] or global states 1 and 2 (GS1 and GS2)[11]. This equilibrium has a central role in the translocation of the bound mRNA and tRNAs in the final step of the elongation cycle[7–11,13].

Cryo-EM studies of PRE complexes have shown that the transition from MS-I to MS-II involves a counterclockwise, ratchet-like rotation of the small ribosomal subunit relative to the large ribosomal subunit (when viewed from the solvent-accessible side of the small subunit)[14]. This rotation, which is accompanied by movement of the L1 stalk on the large subunit toward the small subunit, is coupled to a reconfiguration of the ribosome-bound tRNAs and moves them into a 'hybrid' state in which their acceptor stems are closer to their post-translocation locations[6,15]. Modulation of the transition from MS-I to MS-II by the universally conserved translation factor EF-G is essential for efficient translocation during the elongation cycle[8,11]. The transition from MS-I to MS-II also represents a conceptually attractive point for modulation of the elongation cycle by

[1]Department of Biological Sciences, Columbia University, New York, New York, USA. [2]Northeast Structural Genomics Consortium, Columbia University, New York, New York, USA. [3]Howard Hughes Medical Institute, Department of Biochemistry and Molecular Biophysics, Columbia University, New York, New York, USA. [4]Department of Chemistry, Columbia University, New York, New York, USA. [5]Present address: Department of Physics, Center for the Physics of Living Cells, University of Illinois at Urbana-Champaign, Urbana, Illinois, USA. [6]These authors contributed equally to this work. Correspondence should be addressed to J.F. (jf2192@columbia.edu) or R.L.G. (rlg2118@columbia.edu).

Received 13 May 2013; accepted 21 November 2013; published online 5 January 2014; doi:10.1038/nsmb.2741

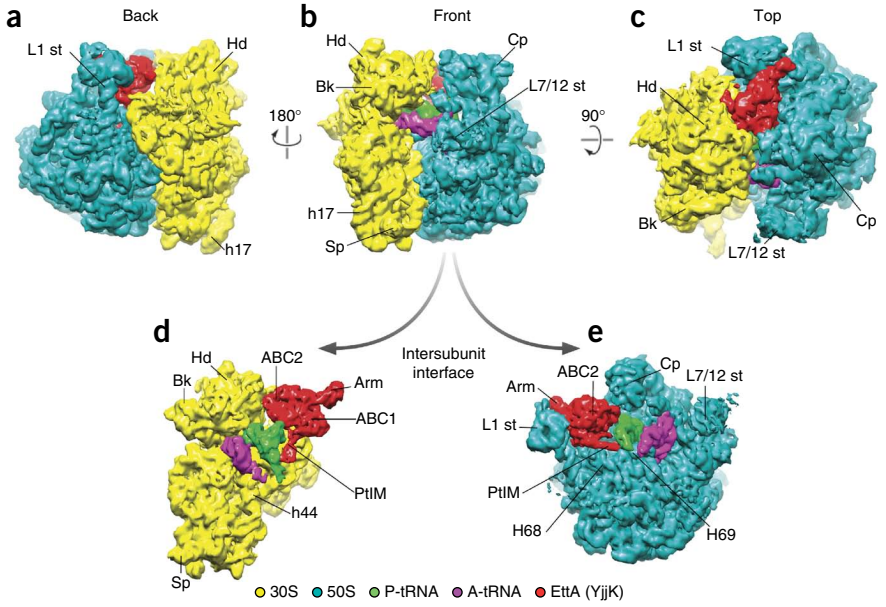

Figure 1 Cryo-EM 3D reconstruction of EttA-EQ2–bound PRE complex. Overview of the segmented cryo-EM map of EttA-EQ2–bound PRE complex reconstructed from class I. (**a**) Back view showing the tRNA-exit site. (**b**) Front view showing the tRNA entry site. (**c**) Top view. (**d**) Intersubunit-interface view from the 50S side, with the 50S subunit computationally removed. (**e**) Intersubunit-interface view from the 30S side, with the 30S subunit computationally removed. A-tRNA, A-site tRNA; P-tRNA, P-site tRNA; hd, 30S-subunit head; bk, 30S-subunit beak; sp, 30S-subunit spur; h17 and h44, helices 17 and 44, respectively, of 16S rRNA; cp, central protuberance of 50S subunit; st, stalk; L7/12 st, stalk formed by proteins L7 and L12; H68 and H69 helices 68 and 69 of 23S rRNA, respectively; ABC, ATP-binding-cassette domain; PtIM, P-site tRNA interaction motif (also called inter–ABC-domain linker of EttA); arm, arm of EttA, an α-helical hairpin in the ABC1 domain of EttA.

regulatory translation factors, but, until now, no such regulatory factor has been demonstrated to act via this mechanism.

Deep understanding of the mechanism by which EF-G drives translocation has been achieved by combining insight from three types of studies. First, elegant biochemical studies have demonstrated that the binding and hydrolysis of GTP by EF-G drives efficient directional translocation on the ribosome[16]. Second, cryo-EM[5,6] and X-ray crystal structures[17] of EF-G complexes with the ribosome have elucidated the structural basis for this activity, which involves stabilization of the ribosomal PRE complex in the MS-II conformation by GTP-bound EF-G. Finally, smFRET studies have characterized the dynamics of the translocation process, revealing that the ribosome undergoes spontaneous fluctuations between the MS-I and MS-II states before EF-G binding[8–11].

The essential eukaryotic and archaeal translation factor ABCE1 (or RLI1) provides another example of the power of synergistic structural and functional studies[18–21]. This protein belongs to the ABC-E family, which represents a different phylogenetic lineage from the ABC-F family within the ATP-binding cassette (ABC) protein superfamily. Cryo-EM studies have shown that ABCE1 (or RLI1) binds near the A site on the ribosome, at the interface between the small and large ribosomal subunits[21], results consistent with its previously demonstrated biochemical activity in dissociating the small and large ribosomal subunits to recycle them from post-termination complexes or stalled ribosomes[18,19]. Combined with X-ray crystal structures of ABCE1 (ref. 22) and model ABC-transporter domains, the cryo-EM structures of ribosome-bound ABCE1 have led to an atomic-resolution model for the mechanism of ABCE1-catalyzed ribosome recycling[21]. ATP binding at the interface between the two ATPase domains in ABCE1 is proposed to drive a mutual rotation of these domains that mechanically pries apart the small and large ribosomal subunits[20,21]. However, interpretation of ribosome structures with some other translation factors has been impeded by uncertainty as to their exact physiological and biochemical activities, as discussed in the **Supplementary Note**.

Boël *et al.*[4] demonstrate that a protein that they renamed EttA (energy-dependent translational throttle A, formerly known as YjjK) gates the entry of 70S ribosomal initiation complex (70S IC) into the translational elongation cycle via a different interaction in the presence of ATP versus ADP[4]. EttA is one of four *E. coli* paralogs belonging to the ABC-F protein family. This phylogenetically distinct lineage within the ABC protein superfamily has multiple representatives in the vast majority of eubacterial genomes and all eukaryotic genomes but very limited prior functional characterization. In this study, we set out to characterize the molecular mechanism of EttA. We used cryo-EM and smFRET to characterize the interaction, with ribosomes, of an EttA variant (EttA-EQ_2) that is locked in the ATP-bound conformation by mutations in the catalytic bases located in its dual ATPase active sites. Our results demonstrate that ATP-bound EttA-EQ_2 binds to the ribosomal E site and kinetically traps the ribosomal PRE complex in the MS-I state. Therefore, EttA regulates translation by modulating the ribosome and tRNA dynamics required for polypeptide elongation. These studies highlight the technical and conceptual advantages of close coordination of functional biochemical experimentation with structural and biophysical studies. This close coordination has provided insight into a sophisticated translational regulatory process at a level of detail and confidence seldom achieved in the past.

RESULTS

The ATP-bound form of EttA binds tightly to the ribosome

We began our structural characterization by using the ATPase-deficient mutant of EttA (EttA-EQ_2), which traps the protein in the ATP-bound conformation, on the basis of extensive evidence summarized in Boël *et al.*[4]. Using *in vivo* Ni^{2+}–nitrilotriacetic acid pulldown experiments (**Supplementary Fig. 1**), we isolated EttA-EQ_2–bound 70S ribosomes at an estimated EttA-EQ_2/70S ribosome molar ratio of ~1:1 from an *E. coli* strain overexpressing N-terminal hexahistidine-tagged EttA-EQ_2 (His_6-EttA-EQ_2). In contrast, we did not detect 70S ribosomes in control pulldown experiments using wild-type His_6-EttA or untagged EttA (**Supplementary Fig. 1**). These results immediately suggested that the interaction of EttA-EQ_2 with 70S ribosome is sufficiently specific and stable for structural characterization of the EttA-EQ_2–bound ribosomal complexes.

Preparation of EttA-EQ_2–bound ribosomal PRE complex

We therefore used cryo-EM[23] and single-particle reconstruction methods[24] to investigate the structure of EttA-EQ_2–bound ribosomal complexes. We used a purified *in vitro* translation system[25] to assemble 70S IC–containing N-formylmethionine (fMet)-bound $tRNA^{fMet}$ on a model mRNA encoding initiator Met-Phe-Lys residues[4]

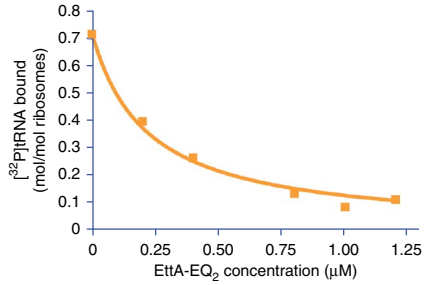

Figure 2 Ribosome E-site binding assay. Filter-binding assay evaluating the influence of increasing concentration of EttA-EQ_2 on the interaction of deacylated [^{32}P]$tRNA^{Phe}$ (0.4 μM) with the E site on 70S ribosomes (0.2 μM) after a 2-min incubation at 4 °C in 20 mM Tris-HCl, pH 7.4, 100 mM NH_4Cl, 10 mM $Mg(OAc)_2$ and 0.1 mM Mg-ATP. The graph shows the fraction of ribosomes retaining an E-site tRNA after three washes on a nitrocellulose filter with 20 mM Tris-HCl, pH 7.4, 100 mM NH_4Cl, 20 mM $Mg(OAc)_2$ and 1 mM EDTA.

(**Supplementary Note**). EttA-EQ_2 together with ATP and the ternary complex Phe-$tRNA^{Phe}$–EF-Tu–GTP were added sequentially to this 70S IC to produce 70S PRE complex. We performed translational activity assays in parallel with cryo-EM sample preparation by using radiolabeled [^{35}S]fMet-$tRNA^{fMet}$ to enable analysis of the peptide products with electrophoretic thin-layer chromatography (eTLC) assays. These assays included EF-G–GTP and Lys-$tRNA^{Lys}$–EF-Tu–GTP to promote translocation and to enable tripeptide synthesis (although we omitted these components from the reactions used to prepare samples for cryo-EM analysis). The translational activity assays yielded ~60% [^{35}S]fMet-Phe dipeptide but only ~10% [^{35}S]fMet-Phe-Lys tripeptide (**Supplementary Fig. 2**), thus confirming the translation activity of the ribosomes and also its inhibition by EttA-EQ_2 (as characterized in Boël *et al.*[4]).

Cryo-EM reconstruction of the EttA-EQ_2–bound PRE complex

After single-particle reconstruction and classification (Online Methods, **Supplementary Note** and **Supplementary Fig. 3**), we obtained a major class comprising 70S ribosomal complexes (class I, 36% of the total data set, 7.5-Å resolution; **Supplementary Fig. 3b**) containing masses of density at the A and P sites that are attributable to A- and P-site tRNAs as well as an additional mass at the E site that is too large to be attributable to a bound tRNA (**Fig. 1**). We assigned this density, on the basis of its size and shape (**Fig. 1d**,**e**), to monomeric EttA-EQ_2. This assignment was confirmed by a standard E-site binding assay[26], which demonstrated that a saturating amount of EttA-EQ_2 almost completely inhibits the binding of deacylated tRNA to the ribosomal E site (**Fig. 2**). On the basis of the aforementioned translational activity assays (**Supplementary Fig. 2**), the ribosome particles in class I represent translation-active ribosomal PRE complex stalled by EttA-EQ_2, which should contain deacylated $tRNA^{fMet}$ at the P site and fMet-Phe-$tRNA^{Phe}$ at the A site. Thus, we assigned the reconstruction from class I to the EttA-EQ_2–bound PRE complex.

The structure of the EttA-EQ_2–bound ribosome derived from the class I density map is similar to that of a PRE complex in MS-I[6,12,27] (**Fig. 3**). However, previous cryo-EM studies on PRE complexes captured two classes of 70S ribosomes that were in MS-I and MS-II conformations, respectively, under similar polyamine-containing, low-Mg^{2+}-concentration buffer conditions and in the absence of translation factors[28]. Therefore, our cryo-EM observation that the EttA-EQ_2–bound PRE complexes homogenously exhibit only the MS-I conformation suggests that EttA-EQ_2 stabilizes 70S ribosome in the MS-I state and prevents the ribosome from advancing to the state required for translocation, an inference validated by smFRET experiments presented below.

Fitting the structure of the EttA-EQ_2–bound PRE complex

To gain more insights into the detailed interactions between EttA-EQ_2 and the bound ribosomal complex, we fitted the atomic structure of the EttA-EQ_2–bound PRE complex into the class I density map by using molecular dynamics flexible fitting (MDFF)[29]. We first built a structural model of monomeric EttA in the ATP-bound conformation by using the crystal structure of nucleotide-free $EttA_2$ (ref. 4). We superimposed the two ABC domains in EttA (ABC1 and

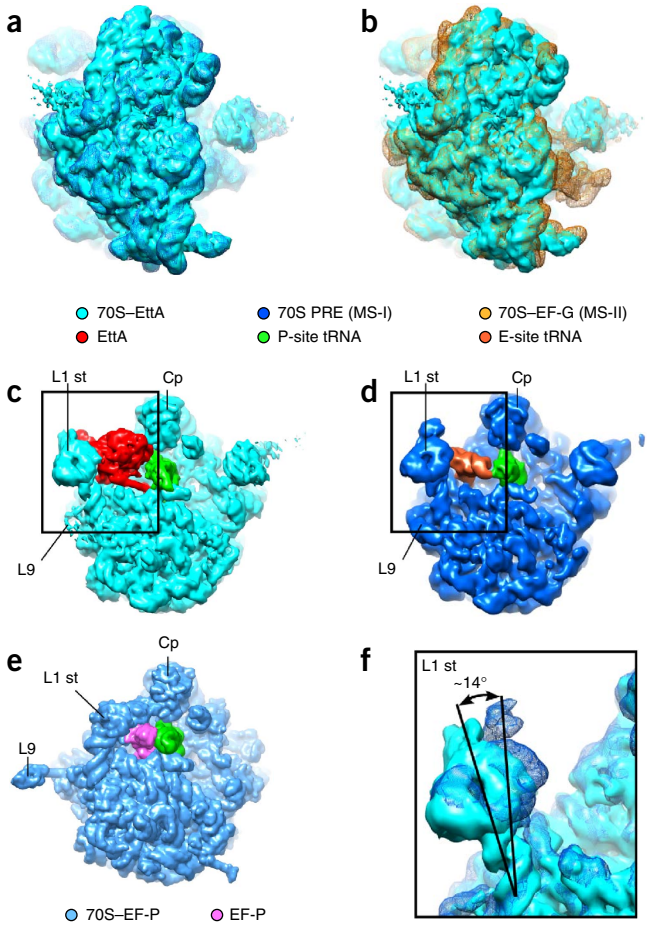

Figure 3 Characterization of the global conformation of EttA-EQ2–bound ribosome. (**a**,**b**) Superimposition of the cryo-EM map of the EttA-EQ2–bound PRE complex determined here on that of the 70S–$tRNA^{fMet}$–MF-$tRNA^{Phe}$ PRE complex in MS-I[6,27] (**a**) or on that of the 70S–MFTI-$tRNA^{Ile}$–EF-G–GDPNP complex with puromycin in MS-II[6] (**b**), as viewed from the solvent side of the 30S subunit. (**c**–**e**) Comparison of EttA's binding site on the 70S ribosome (**c**) with those of E-site tRNA (**d**) and EF-P (**e**), as viewed from the 30S-subunit side of the intersubunit interface. The 30S subunit and A-site tRNA are not shown, to provide clear visualization of the factors and P-site tRNAs. Labels are as in **Figure 1**. (**e**) Map calculated from the X-ray crystal structure of the *T. thermophilus* 70S-ribosome complex with elongation factor EF-P[50], displayed in the same manner and orientation as in **c** and **d**. (**f**) Comparison of the positions of the L1 stalk in the 70S–EttA-EQ_2 and 70S PRE complex, showing superposition of the cryo-EM maps in the boxed regions in **c** and **d**. The maps are colored as in **a**.

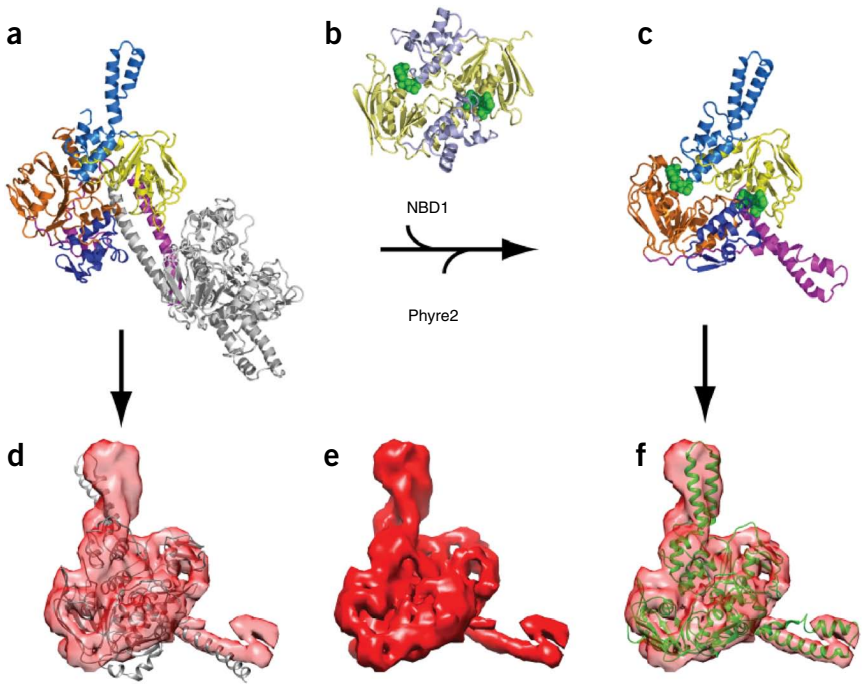

Figure 4 Modeling of ATP-bound EttA monomeric structure and comparison with EttA cryo-EM density map. (**a**–**c**) Modeling of ATP-bound EttA monomeric structure. The crystallographic structure of $EttA_2$ (PDB 4FIN[4]) was cut in half at the inter–ABC-domain linker region (between residues 277 and 278) to generate a monomeric apo-EttA structure model (**a**). Each of the subdomains of the apo-EttA model was aligned to the head-to-tail homodimer structure of ATP-bound CFTR NBD1 (PDB 2PZE[30]) (**b**), and then the missing links were complemented by Phyre2 search hits to yield a monomeric ATP-bound EttA model (**c**). Blue, mechanical coupling subdomain; tan, ATP-binding core; purple, PtIM; gray, the other half of the $EttA_2$ crystallographic structure; green, Mg-ATP. Lighter and darker colors indicate ABC1 and ABC2, respectively. (**d**–**f**) Comparison of the apo-EttA model (**d**) and ATP-bound EttA model (**f**) with the isolated EttA-EQ_2 cryo-EM map (**e**). In **d** and **f**, the cryo-EM map of EttA-EQ_2 was rendered transparent.

ABC2) onto those in the crystal structure of a homologous ABC domain that crystallizes in the form of an ATP-bound homodimer (PDB 2PZE[30]). We performed alignment separately in the F1-like ATP-binding core and the α-helical subdomain of each of the two ABC domains in EttA, in order to account for the subdomain rotation that occurs upon ATP binding to ABC domains[4,31] (Online Methods and **Fig. 4**). After rigid-body fitting of the resulting ATP-bound EttA model into the isolated cryo-EM density corresponding to EttA-EQ_2, we were able to unambiguously assign the two protrusions in the density to unique structural features in EttA relative to other ABC proteins[4]. One of these, the arm (residues 95–139), is an α-helical hairpin extending from the surface of the α-helical subdomain in ABC1, whereas the other, the inter–ABC-domain linker (residues 242–322, named the PtIM below), contains a long α-helical extension at the C terminus of ABC1 (**Fig. 4**). That the similarity of the cryo-EM map is substantially higher to the modeled ATP-bound conformation of EttA than to the conformation observed in its nucleotide-free crystal structure, measured by cross-correlation coefficient, strongly supports the inference that EttA-EQ_2 binds to the ribosome in the standard ATP-bound conformation observed for other ABC domains (Online Methods).

After positioning the ATP-bound model of EttA into the class I density map, we used MDFF to fit into that map the composite atomic structure of the complex containing the 70S ribosome, A-site and P-site tRNAs and EttA (**Supplementary Fig. 4** and Online Methods). In the resulting structure (**Fig. 5**), the ABC1 and ABC2 domains of EttA lie close to the 50S and 30S subunits, respectively. ABC1 contacts helices 68 and 77 of 23S rRNA as well as ribosomal proteins L1 and L33 on the 50S subunit. ABC2 contacts helices 41 and 42 of 16S rRNA as well as ribosomal proteins L5 and L33 on the 50S subunit and ribosomal protein S7 on the 30S subunit (**Fig. 5b**,**d** and **Supplementary Table 1**). The N terminus of EttA is solvent exposed, in agreement with our ability to pull down EttA-EQ2–bound ribosomes via an N-terminal His_6 tag on EttA (**Supplementary Fig. 1**). Notably, the regions of the ABC domains flanking the two nucleotide-binding sites in EttA are also solvent accessible, thus suggesting that EttA should be able to undergo nucleotide exchange while bound to the 70S ribosomal complex.

The arm region of EttA interacts extensively with the L1 stalk of the 50S ribosomal subunit, burying ~1,400 $Å^2$ of surface area on EttA that would otherwise be solvent accessible (**Fig. 3e** and **Supplementary Table 1**). This structural interaction is likely to contribute to the tight binding that is observed between EttA-EQ_2 and the PRE complex and to the putative stabilization of the PRE complex in the MS-I conformation. These inferences are supported by the observation that *E. coli* strains expressing an EttA-EQ_2 variant lacking the arm (EttA-Δarm-EQ_2) do not exhibit the strong *trans*-dominant toxicity phenotype observed in *E. coli* strains expressing full-length EttA-EQ_2 (ref. 4). The conformation of the L1 stalk observed in the EttA-EQ_2–bound ribosome is more open than was previously observed in the MS-I conformation of PRE complexes containing an E-site tRNA[6,27] (**Fig. 3f**). Comparison of these structures indicates that the L1 stalk pivots by ~14° around the hinge region at the base of helix 76 in 23S rRNA, as viewed from the 30S subunit. Moreover, the L1 stalk conformation observed in the EttA-EQ_2–bound PRE complex is similar to the most open L1 stalk conformation that has been observed in the MS-I conformation of PRE complexes lacking an E-site tRNA (class 2 in ref. 32).

EttA-EQ_2 contacts identity elements on the P-site $tRNA^{fMet}$

EttA-EQ_2 bound to the PRE complex has direct access to structural elements in the P-site tRNA that distinguish initiator $tRNA^{fMet}$ from most elongator tRNAs, namely the C1-A72 mismatch (based on tRNA numbering in ref. 33) and the so-called C17pU17a bulge or 'CpU bulge' (described below). The cryo-EM density map (**Fig. 1d**) shows that the side of EttA-EQ_2 facing the P site exhibits a shape that is complementary to the P-site tRNA. The atomic model produced by MDFF fitting of this density map shows direct contact between the inter–ABC-domain linker of EttA-EQ_2 and the aminoacyl-acceptor stem of the P-site tRNA. Notably, the Pfam database[34] identifies the first 70 of the 80 residues in the inter–ABC-domain linker (residues 242–312) as a conserved domain in its own right, which is called PF12484. On this basis, we have designated the inter–ABC-domain linker of EttA as the P-site tRNA interaction motif, PtIM (**Supplementary Fig. 5a**). Some of the conserved residues in the PtIM interact directly with helices 68, 69 and 74 in 23S rRNA as well as with the P-site $tRNA^{fMet}$ (**Supplementary Table 1**), residues that

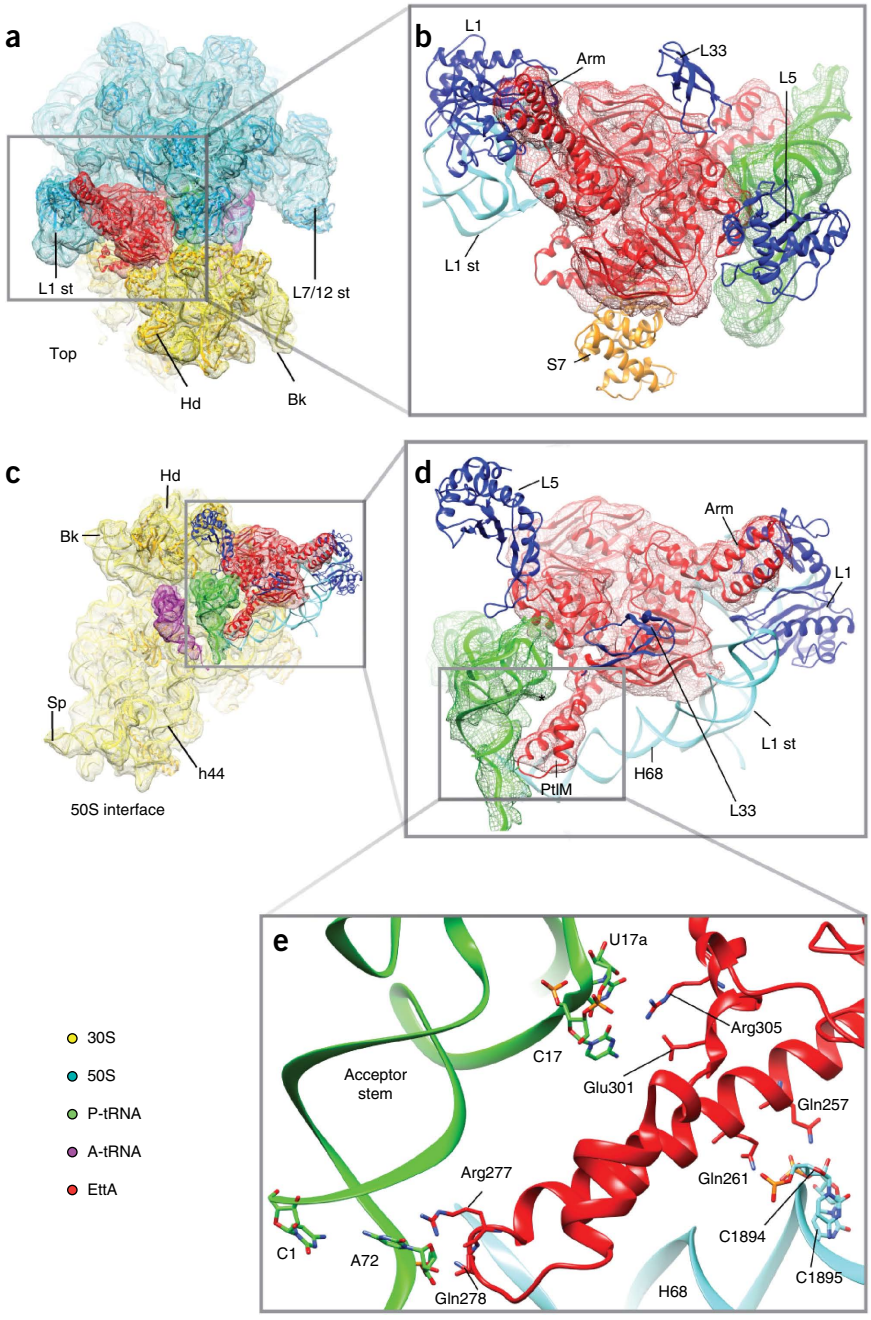

Figure 5 MDFF-fitted EttA-EQ2–bound PRE complex structure. (**a**) Top view. (**b**) Close-up of the boxed region in **a**. (**c**–**e**) Stepwise close-up of the boxed region in **a** viewed from the 50S side of the intersubunit interface. Color scheme as in **Figure 1**. Blue and orange ribbons, ribosomal proteins of 50S and 30S subunit, respectively. The cryo-EM map is rendered as mesh contour. The asterisked region in **d** indicates the protrusion formed by the CpU bulge of P-site tRNA^{fMet}. Residues involved in possible interactions between EttA and P-site tRNA^{fMet} or 23S rRNA are represented as sticks in **e**.

seem likely to stabilize the observed conformation of the PtIM. Analysis of the class III cryo-EM map, obtained from ribosome particle classification, support this hypothesis. The class III map contains density for EttA but not for tRNA molecules in either the P or A site on the ribosome (**Supplementary Fig. 6** and **Supplementary Note**). In these tRNA-free particles, the EttA density is substantially weaker in the region of the PtIM connected to ABC2 compared to the density in the same region of EttA in the class I map, which has tRNA molecules bound in both the A and the P site (comparison of **Fig. 1** and **Supplementary Fig. 6**). These observations suggest that PtIM makes functionally important stabilizing interactions with the P-site tRNA, in the absence of which the PtIM fails to adopt a well-defined conformation when EttA is bound to ribosomes.

The C1-A72 mismatch at the end of the aminoacyl-acceptor stem is a structural feature that distinguishes initiator tRNA^{fMet} from most elongator tRNAs[35] (**Supplementary Fig. 5b**). In the MDFF-fitted structure of the EttA-EQ$_2$–bound PRE complex, the aminoacyl-acceptor stem of tRNA^{fMet} interacts with several positively charged residues at the distal end of the PtIM (residues 275–286), including Arg277 and Lys281 (**Fig. 5e** and **Supplementary Table 1**). Another distinguishing feature of tRNA^{fMet} is the CpU bulge within the dihydrouridine loop (D loop)[33], which comprises bases C17 and U17a (where '17a' refers to an additional nucleotide between 17 and 18). This feature is present in both isoforms of initiator tRNA^{fMet} as well as in two of three isoforms of tRNA^{Pro} in *E. coli* but is absent from all other elongator tRNAs (**Supplementary Fig. 5b**). The two bases of the CpU bulge are flipped out of the elbow region of the tRNA in crystal structures of *E. coli* tRNA^{fMet} either alone[36] or bound at the P site of the *Thermus thermophilus* 70S ribosome[37]. In the class I density map, this bulge is prominent in the P-site tRNA but missing in the A-site tRNA (**Figs. 1d** and **5d**), observations consistent with the assignment of tRNA^{fMet} at the P site and tRNA^{Phe} at the A site. Several residues in EttA-EQ$_2$, including residues 299–302 in PtIM and a region on the surface of ABC2, may interact with the CpU bulge of tRNA^{fMet} (**Supplementary Table 1**). Taken together, the interactions of EttA-EQ$_2$ with the aminoacyl-acceptor stem and the CpU bulge of tRNA^{fMet} suggest that EttA is capable of interacting more strongly with ribosomes bearing tRNA^{fMet} rather than elongator tRNAs in the P site, an inference consistent with biochemical assays presented in Boël *et al.* showing that EttA interacts preferentially with the 70S IC compared to ribosomes that have entered the elongation cycle[4].

EttA-EQ$_2$ binding restricts ribosome and tRNA dynamics

To explore the mechanism through which EttA's interactions with the 70S ribosome and the P-site tRNA regulate protein synthesis, we turned to smFRET experiments (**Fig. 6**). These experiments have been used extensively to characterize how translation factors modulate the dynamics of 70S ribosomal complexes as part of the mechanisms through which they regulate translation[8,10,11,38,39]. We conducted initial experiments by using a previously developed smFRET signal between the L1 stalk and a deacylated P-site tRNA^{Phe}

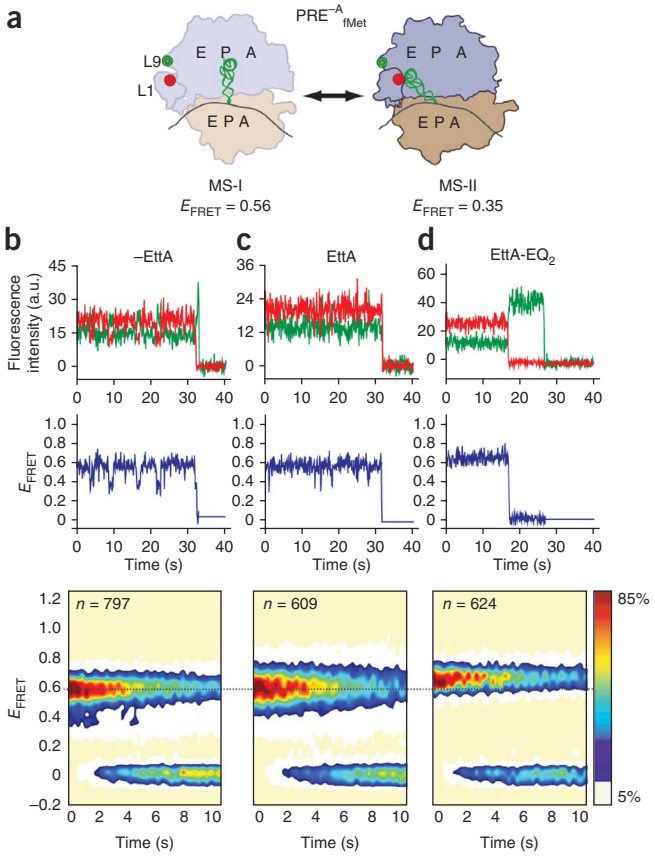

Figure 6 EttA-mediated regulation of the open L1 stalk↔closed L1 stalk equilibrium of a PRE$^{-A}_{fMet}$ complex as shown by smFRET$_{L1\text{-}L9}$. (**a**) Cartoon diagram of the conformational equilibrium of the PRE$^{-A}_{fMet}$ complex between the MS-I conformation containing an open L1 stalk (left) and the MS-II conformation containing a closed L1 stalk (right). Tan cartoon, 30S subunit; blue cartoon, 50S subunit; green ribbon, tRNA^{fMet}; black curve, mRNA; green circle, Cy3 FRET donor fluorophore; red circle, Cy5 FRET acceptor fluorophore. (**b**–**d**) smFRET$_{L1\text{-}L9}$ experiments recorded in the presence of 2 mM ATP and in the absence of EttA (**b**), in the presence of 6 μM EttA (**c**) or in the presence of 6 μM EttA-EQ$_2$ (**d**). Top, representative Cy3 and Cy5 fluorescence intensity trajectories over time. The fluorescence intensities are plotted in arbitrary units (a.u.) with the Cy3 fluorescence intensity plotted in green and the Cy5 fluorescence intensity plotted in red. Middle, corresponding E_{FRET} trajectories over time. The E_{FRET} at each time point was calculated by $E_{FRET} = I_{Cy5}/(I_{Cy3} + I_{Cy5})$, where I_{Cy3} and I_{Cy5} are emission intensities of Cy3 and Cy5, respectively, and is plotted in blue. Bottom, surface contour plots of the time evolution of the population FRET. The contour plots were generated by superimposition of individual E_{FRET} trajectories over time and are colored from white (lowest populated) to red (highest populated). *n*, number of trajectories used to construct each contour plot.

(smFRET$_{L1\text{-}tRNA}$)[11] in a ribosomal PRE complex analog with an empty A site (PRE$^{-A}_{Phe}$). Control smFRET$_{L1\text{-}tRNA}$ experiments recorded in the absence of EttA-EQ$_2$ exhibited fluctuations between FRET states centered at a FRET efficiency (E_{FRET}) = 0.15, associated with MS-I, and E_{FRET} = 0.74, associated with MS-II (**Supplementary Fig. 7**, **Supplementary Table 2** and Online Methods). In contrast, smFRET$_{L1\text{-}tRNA}$ experiments recorded in the presence of 1.8 μM EttA-EQ$_2$ and 2 mM ATP showed a dramatic shift in the MS-I↔MS-II equilibrium of the PRE$^{-A}_{Phe}$ complex to a FRET state centered at E_{FRET} = 0.15, consistently with stabilization of the ribosome in MS-I by EttA-EQ$_2$ in the presence of ATP.

To more sensitively and directly investigate the conformational dynamics of the L1 stalk, we next used a previously described smFRET signal between the apical tip and the base of the L1 stalk (smFRET$_{L1\text{-}L9}$)[10] in a PRE^{-A} complex containing a deacylated P-site tRNA^{fMet} and an empty A site (PRE$^{-A}_{fMet}$) (**Fig. 6**, **Supplementary Table 2** and Online Methods). Control experiments recorded in the absence of EttA or EttA-EQ$_2$ exhibited fluctuations between FRET states centered at E_{FRET} = 0.56, associated with the open L1 stalk in MS-I, and E_{FRET} = 0.35, associated with the closed L1 stalk in MS-II. In contrast, smFRET$_{L1\text{-}L9}$ experiments recorded in the presence of 6 μM EttA (i.e., the wild-type protein) and 2 mM ATP showed exclusive population of the FRET state centered at E_{FRET} = 0.56, demonstrating that EttA shifts the conformational equilibrium of the ribosome toward the MS-I state with an open conformation of the L1 stalk. Experiments recorded in the presence of 6 μM EttA-EQ$_2$ and 2 mM ATP demonstrated an even stronger effect, with shifting of the open L1 stalk↔closed L1 stalk equilibrium toward a FRET state centered at E_{FRET} = 0.62 that is even higher than the E_{FRET} observed for the open L1 stalk in MS-I. This result suggests that EttA-EQ$_2$ stabilizes a conformation of the L1 stalk in which the mean separation between the labeling positions on ribosomal proteins L1 and L9 is slightly shorter than that observed for the open L1 stalk in MS-I, conclusions consistent with those from our cryo-EM studies.

DISCUSSION

We propose, on the basis of the work reported here and in Boël *et al.*[4], a model for the regulation of translation by EttA at the start of the elongation cycle (**Fig. 7**). ATP-bound EttA docks initially to the E site of a 70S IC. Upon accommodation of an aminoacylated tRNA in the A site of this complex, the ATP-bound form of EttA stimulates peptide-bond formation[4] by modulating the conformation of the PTC on the ribosome, thus resulting in formation of a 70S PRE complex, which is stabilized in the MS-I state by EttA. Modulation of the conformation of the PTC is mediated by the interactions of EttA with ribosomal proteins, rRNA and the acceptor stem of the P-site tRNA, which is proximal to the PTC. The ATPase activity assays presented in Boël *et al.*[4] suggest that these EttA-ribosome interactions reciprocally stimulate ATP hydrolysis by EttA. ATP hydrolysis by EttA is hypothesized to drive the two ABC domains apart[40] into a conformation that is no longer compatible with ribosome binding, thereby triggering release of EttA. After EttA's dissociation, the PRE complex regains the capability to undergo MS-I↔MS-II transitions, thereby permitting EF-G binding and translocation to occur and completing the process by which EttA gates entry of the 70S IC into the translational elongation cycle. In contrast, the ATPase-deficient EttA-EQ$_2$ mutant protein, which is trapped in the ATP-bound conformation, remains bound to the PRE complex and keeps it stalled in MS-I.

The cryo-EM structure shows that the arm and the toe of EttA—structural elements found in EttA and other ABC-F proteins but not in other ABC superfamily proteins—both contact structural elements of the large ribosomal subunit within the 70S PRE complex (**Fig. 5b**,**d** and **Supplementary Table 1**). Specifically, the arm of EttA makes extensive contacts with the L1 stalk of the large ribosomal subunit while the toe of EttA contacts the ribosomal protein L5. The functional importance of the observed interaction of EttA's arm with the L1 stalk of the ribosome is supported by genetic complementation experiments presented in Boël *et al.*[4]. The cryo-EM structure reported here verifies the inference in Boël *et al.*[4], based on the crystal structure of EttA, that these structural elements unique to ABC-F proteins mediate contact with some functional interaction partner. The crystal structure of EttA reported in Boël *et al.*[4] shows that these structural

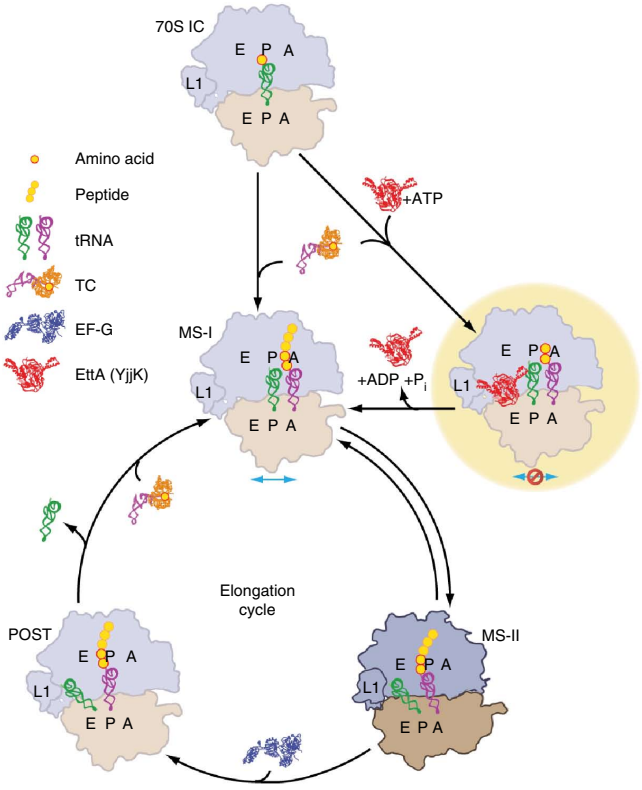

Figure 7 Schematic model of the influence of EttA, in the presence of ATP, on the early steps in protein synthesis on the ribosome. For simplicity, not all intermediate steps in translation are shown; more details are in text. Tan, 30S; blue, 50S; orange, EF-Tu; 70S IC, 70S ribosomal initiation complex; TC, aminoacyl-tRNA–EF-Tu–GTP ternary complex. Three yellow dots in tandem represent the heading peptide, excluding the two most recently added amino acids (red circles). Blue arrow indicates the propensity of PRE complexes for spontaneous ratchet-like intersubunit rotation. Red stop sign symbolizes the inhibition of the MS-I↔MS-II dynamics by the binding of the ATP-bound form of EttA to the ribosomal E site. EttA-mediated translation regulation in the presence of ADP, described by Boël *et al.*[4], is not represented in this schematic. P_i, inorganic phosphate; POST, post-translocational complex.

elements are inserted at the sites at which ABC domains contact the transmembrane domains in ABC transporters[41–43]. Notably, a chromodomain inserted in the equivalent loop in the second ABC domain of eEF3 mediates interaction with a different region of the ribosome[44].

On the basis of the peripheral, solvent-exposed location of the ATP-binding sites in EttA in the ribosome-bound structure reported here, nucleotide exchange on EttA should be able to occur while EttA remains bound to the ribosome. The monomer structure fit to the cryo-EM map shows closure of the interface between ABC1 and ABC2, as compared to the nucleotide-free crystal structure of EttA[4], that yields a conformation in which the two ABC domains interact in a geometry equivalent to that observed in a wide variety of other ATP-bound ABC proteins (including that in the crystal structure of the E-to-Q mutant of MJ0796)[40,43,45,46]. This structural observation supports the inference made in Boël *et al.*[4], based on results obtained with a wide variety of ABC proteins, that the EQ_2 mutations trap EttA in an ATP-bound conformation.

Specific structural interactions between EttA and the P-site tRNA visualized in the cryo-EM structure reported in this paper could contribute to the specificity of EttA for the 70S IC compared to elongating ribosomes[4]. The PtIM and ABC2 domains of EttA interact with two distinguishing structural features of initiator $tRNA^{fMet}$, the C1-A72 mismatch and the CpU bulge, the first of which does not occur in any other tRNA and the second of which occurs in only some isoforms of $tRNA^{Pro}$. Notably, there are several parallels between the mechanism proposed here for EttA and that previously proposed for the elongation factor EF-P[47]. Both EF-P[47] and EttA[4] have been proposed to modulate the conformation of the PTC to control the peptidyl-transferase activity of the ribosome when a tRNA containing the CpU bulge is bound in the P site, as discussed in the **Supplementary Note**.

Boël *et al.*[4] also present evidence that, in the presence of ADP, EttA stabilizes the 70S IC in a hibernating state that prevents synthesis of the first peptide bond on the ribosome[4]. The cryo-EM structure reported here helps guide development of an integrated model for this activity and the functional interaction of EttA with 70S IC. The global conformation of the ribosome in the hibernating state stabilized by EttA in the presence of ADP is likely to be similar to that of the EttA-EQ2–bound PRE complex in the presence of ATP reported in this paper, but it must have important local conformational differences in the vicinity of the PTC to inhibit, rather than promote, peptide-bond formation. The lifetime of this hibernating state is likely to be longer than the lifetime of the state stabilized by EttA in the presence of ATP because in the latter state, ATP hydrolysis by EttA presumably promotes a conformational change of EttA accelerating its release from the ribosome. In the absence of this driving force produced by ATP hydrolysis, EttA in the presence of ADP presumably remains bound to the ribosome longer. Our cryo-EM structure suggests that nucleotide exchange could take place on EttA while it remains bound to the ribosome. Upon binding ATP, ribosome-bound EttA should drive peptide-bond formation. EttA would then be rapidly released from the ribosome upon ATP hydrolysis (**Fig. 7**), which would induce escape of the ribosome from the hibernating state stabilized by EttA in the presence of ADP. In contrast, under conditions of energy depletion, which results in an elevated concentration of ADP compared to ATP[48,49], competition of ADP with ATP for interaction with the ATPase active sites in ribosome-bound EttA could perpetuate the hibernating state and prevent the ribosome from entering the translation elongation cycle. This model for the mechanism of nucleotide exchange and ATP hydrolysis by ribosome-bound EttA, while consistent with the biochemical results presented by Boël *et al.*[4] and the cryo-EM structure presented here, must be critically evaluated in future research on this system.

In conclusion, the research reported in this paper demonstrates that the ATP-bound form of EttA interacts with the E site of the 70S ribosome in the MS-I state and modulates the transition of the translating ribosome from MS-I to MS-II. This molecular mechanism used by EttA is new among those of all the known translational regulatory factors. Future work is needed to validate EttA's specificity for ribosomes with an initiator $tRNA^{fMet}$ in the P site and to provide more details on the mechanism of ATP hydrolysis on the ribosome-bound EttA. The methods used to characterize EttA in this paper and in Boël *et al.*[4] provide a paradigm to evaluate whether translation is modulated in a related manner by other established and putative translation factors, including the many uncharacterized proteins in the ABC-F protein family (for example, Uup, YbiT and YheS in *E. coli*).

METHODS

Methods and any associated references are available in the online version of the paper.

Accession codes. The EM maps have been deposited in the Electron Microscopy Data Bank under accession codes EMD-5784 (class I), EMD-5785 (class II) and EMD-5786 (class III). Coordinates of the EM-based model for class I have been deposited in the Protein Data Bank under accession number 3J5S.

Note: Any Supplementary Information and Source Data files are available in the online version of the paper.

ACKNOWLEDGMENTS

This work was supported by Howard Hughes Medical Institute and US National Institutes of Health (NIH) grants (R01 GM29169 and GM55440) to J.F.; an NIH grant (2U54 GM074958) and a US National Science Foundation (NSF) grant (0424043) to J.F.H.; a Burroughs Wellcome Fund Career Awards in the Biomedical Sciences (CABS 1004856), an NSF CAREER Award (MCB 0644262) and an NIH National Institute of General Medical Sciences grant (R01 GM084288) to R.L.G. The authors thank R.A. Grassucci for assistance with cryo-EM data collection and M. Thomas and C. Kinz-Thompson for assistance with the preparation of illustrations. We thank members of the Frank, Hunt and Gonzalez laboratories for advice and technical assistance.

AUTHOR CONTRIBUTIONS

G.B., B.C., J. Fei, J.F.H., R.L.G. and J. Frank designed the experiments. G.B. performed biochemical studies and prepared the biological samples for cryo-EM. B.C. collected cryo-EM data and performed 3D reconstruction. Y.H., B.C. and C.W. performed the modeling, fitting and analysis. W.N. and J. Fei collected and analyzed smFRET data. B.C., G.B., Y.H., W.N., R.L.G., J.F.H. and J. Frank wrote the manuscript; all authors approved the final manuscript.

COMPETING FINANCIAL INTERESTS

The authors declare no competing financial interests.

1. Wilson, D.N. & Nierhaus, K.H. The weird and wonderful world of bacterial ribosome regulation. *Crit. Rev. Biochem. Mol. Biol.* **42**, 187–219 (2007).
2. Schmeing, T.M. & Ramakrishnan, V. What recent ribosome structures have revealed about the mechanism of translation. *Nature* **461**, 1234–1242 (2009).
3. Steitz, T.A. A structural understanding of the dynamic ribosome machine. *Nat. Rev. Mol. Cell Biol.* **9**, 242–253 (2008).
4. Boël, G. *et al.* The ABC-F protein EttA gates ribosome entry into the translation elongation cycle. *Nat. Struct. Mol. Biol.* doi:10.1038/nsmb.2740 (5 January 2014).
5. Agrawal, R.K., Heagle, A.B., Penczek, P., Grassucci, R.A. & Frank, J. EF-G-dependent GTP hydrolysis induces translocation accompanied by large conformational changes in the 70S ribosome. *Nat. Struct. Biol.* **6**, 643–647 (1999).
6. Valle, M. *et al.* Locking and unlocking of ribosomal motions. *Cell* **114**, 123–134 (2003).
7. Blanchard, S.C., Kim, H.D., Gonzalez, R.L., Puglisi, J.D. & Chu, S. tRNA dynamics on the ribosome during translation. *Proc. Natl. Acad. Sci. USA* **101**, 12893–12898 (2004).
8. Cornish, P.V., Ermolenko, D.N., Noller, H.F. & Ha, T. Spontaneous intersubunit rotation in single ribosomes. *Mol. Cell* **30**, 578–588 (2008).
9. Cornish, P.V. *et al.* Following movement of the L1 stalk between three functional states in single ribosomes. *Proc. Natl. Acad. Sci. USA* **106**, 2571–2576 (2009).
10. Fei, J. *et al.* Allosteric collaboration between elongation factor G and the ribosomal L1 stalk directs tRNA movements during translation. *Proc. Natl. Acad. Sci. USA* **106**, 15702–15707 (2009).
11. Fei, J., Kosuri, P., MacDougall, D.D. & Gonzalez, R.L. Coupling of ribosomal L1 stalk and tRNA dynamics during translation elongation. *Mol. Cell* **30**, 348–359 (2008).
12. Frank, J., Gao, H., Sengupta, J., Gao, N. & Taylor, D.J. The process of mRNA-tRNA translocation. *Proc. Natl. Acad. Sci. USA* **104**, 19671–19678 (2007).
13. Kim, H.D., Puglisi, J.D. & Chu, S. Fluctuations of transfer RNAs between classical and hybrid states. *Biophys. J.* **93**, 3575–3582 (2007).
14. Frank, J. & Agrawal, R.K. A ratchet-like inter-subunit reorganization of the ribosome during translocation. *Nature* **406**, 318–322 (2000).
15. Agrawal, R.K. *et al.* Visualization of tRNA movements on the *Escherichia coli* 70S ribosome during the elongation cycle. *J. Cell Biol.* **150**, 447–460 (2000).
16. Spirin, A.S. in *Prog. Nucleic Acid Res. Mol. Biol.* Vol. 32 (eds. Waldo, E.C. & Kivie, M.) 75–114 (Academic Press, 1985).
17. Gao, Y.-G. *et al.* The structure of the ribosome with elongation factor G trapped in the posttranslocational state. *Science* **326**, 694–699 (2009).
18. Pisarev, A.V. *et al.* The role of ABCE1 in eukaryotic posttermination ribosomal recycling. *Mol. Cell* **37**, 196–210 (2010).
19. Khoshnevis, S. *et al.* The iron-sulphur protein RNase L inhibitor functions in translation termination. *EMBO Rep.* **11**, 214–219 (2010).
20. Barthelme, D. *et al.* Ribosome recycling depends on a mechanistic link between the FeS cluster domain and a conformational switch of the twin-ATPase ABCE1. *Proc. Natl. Acad. Sci. USA* **108**, 3228–3233 (2011).
21. Becker, T. *et al.* Structural basis of highly conserved ribosome recycling in eukaryotes and archaea. *Nature* **482**, 501–506 (2012).
22. Karcher, A., Schele, A. & Hopfner, K.-P. X-ray structure of the complete ABC enzyme ABCE1 from *Pyrococcus abyssi*. *J. Biol. Chem.* **283**, 7962–7971 (2008).
23. Grassucci, R.A., Taylor, D. & Frank, J. Visualization of macromolecular complexes using cryo-electron microscopy with FEI Tecnai transmission electron microscopes. *Nat. Protoc.* **3**, 330–339 (2008).
24. Frank, J. *Three-dimensional electron microscopy of macromolecular assemblies: visualization of biological molecules in their native state* (Oxford Univ. Press, 2006).
25. Fei, J. *et al.* A highly purified, fluorescently labeled *in vitro* translation system for single-molecule studies of protein synthesis. *Methods Enzymol.* **472**, 221–259 (2010).
26. Grajevskaja, R.A., Ivanov, Y.V. & Saminsky, E.M. 70-S ribosomes of *Escherichia coli* have an additional site for deacylated tRNA binding. *Eur. J. Biochem.* **128**, 47–52 (1982).
27. Valle, M. *et al.* Incorporation of aminoacyl-tRNA into the ribosome as seen by cryo-electron microscopy. *Nat. Struct. Biol.* **10**, 899–906 (2003).
28. Agirrezabala, X. *et al.* Visualization of the hybrid state of tRNA binding promoted by spontaneous ratcheting of the ratcheting ribosome. *Mol. Cell* **32**, 190–197 (2008).
29. Trabuco, L.G., Villa, E., Mitra, K., Frank, J. & Schulten, K. Flexible fitting of atomic structures into electron microscopy maps using molecular dynamics. *Structure* **16**, 673–683 (2008).
30. Atwell, S. *et al.* Structures of a minimal human CFTR first nucleotide-binding domain as a monomer, head-to-tail homodimer, and pathogenic mutant. *Protein Eng. Des. Sel.* **23**, 375–384 (2010).
31. Karpowich, N. *et al.* Crystal structures of the MJ1267 ATP binding cassette reveal an induced-fit effect at the ATPase cctive site of an ABC transporter. *Structure* **9**, 571–586 (2001).
32. Agirrezabala, X. *et al.* Structural characterization of mRNA-tRNA translocation intermediates. *Proc. Natl. Acad. Sci. USA* **109**, 6094–6099 (2012).
33. Steinberg, S., Misch, A. & Sprinzl, M. Compilation of tRNA sequences and sequences of tRNA genes. *Nucleic Acids Res.* **21**, 3011–3015 (1993).
34. Finn, R.D. *et al.* The Pfam protein families database. *Nucleic Acids Res.* **38**, D211–D222 (2010).
35. Laursen, B.S., Sorensen, H.P., Mortensen, K.K. & Sperling-Petersen, H.U. Initiation of protein synthesis in bacteria. *Microbiol. Mol. Biol. Rev.* **69**, 101–123 (2005).
36. Barraud, P., Schmitt, E., Mechulam, Y., Dardel, F. & Tisné, C. A unique conformation of the anticodon stem-loop is associated with the capacity of $tRNA^{fMet}$ to initiate protein synthesis. *Nucleic Acids Res.* **36**, 4894–4901 (2008).
37. Voorhees, R.M., Weixlbaumer, A., Loakes, D., Kelley, A.C. & Ramakrishnan, V. Insights into substrate stabilization from snapshots of the peptidyl transferase center of the intact 70S ribosome. *Nat. Struct. Mol. Biol.* **16**, 528–533 (2009).
38. Marshall, R.A., Aitken, C.E. & Puglisi, J.D. GTP hydrolysis by IF2 guides progression of the ribosome into elongation. *Mol. Cell* **35**, 37–47 (2009).
39. Sternberg, S.H., Fei, J., Prywes, N., McGrath, K.A. & Gonzalez, R.L. Translation factors direct intrinsic ribosome dynamics during translation termination and ribosome recycling. *Nat. Struct. Mol. Biol.* **16**, 861–868 (2009).
40. Smith, P.C. *et al.* ATP binding to the motor domain from an ABC transporter drives formation of a nucleotide sandwich dimer. *Mol. Cell* **10**, 139–149 (2002).
41. Davidson, A.L., Dassa, E., Orelle, C. & Chen, J. Structure, function, and evolution of bacterial ATP-binding cassette systems. *Microbiol. Mol. Biol. Rev.* **72**, 317–364 (2008).
42. Dawson, R.J. & Locher, K.P. Structure of a bacterial multidrug ABC transporter. *Nature* **443**, 180–185 (2006).
43. Oldham, M.L. & Chen, J. Crystal structure of the maltose transporter in a pretranslocation intermediate state. *Science* **332**, 1202 (2011).
44. Andersen, C.B.F. *et al.* Structure of eEF3 and the mechanism of transfer RNA release from the E-site. *Nature* **443**, 663–668 (2006).
45. Hopfner, K.-P. *et al.* Structural biology of Rad50 ATPase: ATP-driven conformational control in DNA double-strand break repair and the ABC-ATPase superfamily. *Cell* **101**, 789–800 (2000).
46. Vergani, P., Lockless, S.W., Nairn, A.C. & Gadsby, D.C. CFTR channel opening by ATP-driven tight dimerization of its nucleotide-binding domains. *Nature* **433**, 876–880 (2005).
47. Doerfel, L.K. *et al.* EF-P is essential for rapid synthesis of proteins containing consecutive proline residues. *Science* **339**, 85–88 (2013).
48. Buckstein, M.H., He, J. & Rubin, H. Characterization of nucleotide pools as a function of physiological state in *Escherichia coli*. *J. Bacteriol.* **190**, 718–726 (2008).
49. Chapman, A.G., Fall, L. & Atkinson, D.E. Adenylate energy charge in *Escherichia coli* during growth and starvation. *J. Bacteriol.* **108**, 1072–1086 (1971).
50. Blaha, G., Stanley, R.E. & Steitz, T.A. Formation of the first peptide bond: the structure of EF-P bound to the 70S ribosome. *Science* **325**, 966–970 (2009).

ONLINE METHODS

Pulldown of 70S ribosome with His_6-EttA-EQ_2. These methods are described in the **Supplementary Note**.

smFRET experiments on PRE$^{-A}_{fMet}$ and PRE$^{-A}_{Phe}$ complexes. smFRET experiments were performed with a laboratory-built total internal reflection fluorescence (TIRF) microscope as previously described[10,11,51] in a Tris-Polymix buffer containing 50 mM Tris acetate, pH 7.0 at 25 °C, 100 mM KCl, 5 mM NH_4OAc, 15 mM $Mg(OAc)_2$, 0.5 mM $Ca(OAc)_2$, 0.1 mM EDTA, 10 mM 2-mercaptoethanol, 5 mM putrescine dihydrochloride and 1 mM spermidine (free base) that was supplemented with an oxygen-scavenging system (2.5 mM 3,4-dihydroxybenzoic acid (PCA), 25 nM protocatechuate 3,4-dioxygenase (PCD), and 1% (w/v) β-D-glucose).

The PRE$^{-A}_{Phe}$ complex used for the smFRET$_{L1\text{-}tRNA}$ experiments was prepared with a ribosome labeled with a Cy5 FRET acceptor fluorophore at ribosomal protein L1 and a P-site tRNA^{Phe} labeled with a Cy3 FRET donor fluorophore at the central-fold domain as previously described[11], where it was designated as the PRE-2 complex. We note that tRNA^{Phe}, rather than tRNA^{fMet}, was used for these experiments because the labeling position within the central-fold domain of tRNA^{Phe} provides an smFRET$_{L1\text{-}tRNA}$ signal that has greater dynamic range, and therefore greater sensitivity, than does the smFRET$_{L1\text{-}tRNA}$ signal corresponding to the labeling position in the central-fold domain of tRNA^{fMet} [10].

The PRE$^{-A}_{fMet}$ complex used for the smFRET$_{L1\text{-}L9}$ experiments was prepared with ribosomes labeled with a Cy5 FRET acceptor fluorophore at ribosomal protein L1 within the apical tip of the L1 stalk and with a Cy3 FRET donor fluorophore at ribosomal protein L9 protein within the base of the L1 stalk as previously described in ref. 51, where it was designated as the PRE$^{-A}_{fMet1}$ complex.

smFRET$_{L1\text{-}tRNA}$ experiments were performed by preparation of samples containing (i) 100 pM PRE$^{-A}_{fMet}$ complex; (ii) 100 pM PRE$^{-A}_{fMet}$ complex, 1.8 μM wild-type EttA and 0.8 mM Mg-ATP; or (iii) 100 pM PRE$^{-A}_{fMet}$, 1.8 μM ATPase-deficient mutant EttA-EQ_2, and 0.8 mM Mg-ATP in Tris-Polymix buffer, with incubation of each sample for 2 min at 25 °C, loading of each sample into an imaging flow cell and imaging of each flow cell as previously described[11]. smFRET$_{L1\text{-}l9}$ experiments were performed by preparation of samples containing (i) 100 pM PRE$^{-A}_{fMet}$ complex; (ii) 100 pM PRE$^{-A}_{fMet}$ complex, 6 μM wild-type EttA and 2 mM Mg-ATP; or (iii) 100 pM PRE$^{-A}_{fMet}$, 6 μM ATPase-deficient mutant EttA-EQ_2 and 2 mM Mg-ATP in Tris-Polymix buffer, with incubation of each sample for 2 min at 25 °C, loading of each sample into an imaging flow cell and imaging of each flow cell as previously described[51].

The fractional populations of MS-I and MS-II, equilibrium constants governing the MS-I↔MS-II equilibrium, and the transition rates between MS-I and MS-II reported for the PRE$^{-A}_{fMet}$ and PRE$^{-A}_{Phe}$ complexes in **Supplementary Table 2** were calculated according to previously described protocols[10,11,51].

Cryo-EM sample preparation and peptide formation assay. The pT7gp32 mRNA, containing the first four codons AUG-UUU-AAA-GAA (Met-Phe-Lys-Glu), was produced as described by Fei *et al.*[25]. The pT7gp32.1–20 plasmid was used as a template for the mRNA. This plasmid is a derivate from the pT7gp32.1–224 plasmid and has a stop codon after residue 20.

Peptide formation assay. All the components and proteins for the *in vitro* translation were prepared and purified exactly as described in the method of Fei *et al.*[25]. The [^{35}S]fMet-tRNA^{fMet} was prepared with the same protocol but with the methionine replaced by 3 μM of [^{35}S]methionine (PerkinElmer) and quenched 5 min after the beginning of the reaction with 16 μM of cold methionine. Estimation of aminoacylation-to-formylation yields was assessed by hydrophobic interaction chromatography[25]. The translation was done in Polymix buffer with 3.5 mM $Mg(OAc)_2$ (50 mM Tris acetate, pH 6.9, 100 mM KCl, 5 mM NH_4OAc, 3.5 mM $Mg(OAc)_2$, 0.5 mM $Ca(OAc)_2$, 0.1 mM EDTA, 1 mM spermidine, 5 mM putrescine and 6 mM 2-mercaptoethanol) containing 0.5 mM Mg-ATP. Reactions were performed at 37 °C except as otherwise indicated, with the following concentrations: mRNA (1.7 μM), [^{35}S]fMet-tRNA^{fMet} (0.3 μM), 70S ribosome (0.45 μM), the initiation factors IF1, IF2 and IF3 (~0.5 μM each), the corresponding aminoacyl-tRNA (0.7 μM) and the elongation factors (EF-Tu (2 μM), EF-Ts (1 μM), and EF-G (1.5 μM)). The 70S IC was assembled by incubation of 70S ribosome with IF1, IF2, IF3 and GTP in Polymix buffer with 3.5 mM $Mg(OAc)_2$ for 10 min, then with the mRNA for 10 min and then with [^{35}S]fMet-tRNA^{fMet} for 10 min. After that, the 70S IC was kept on ice for at least 10 min before being used for the elongation reactions. EF-G and ternary complexes (Phe-tRNA^{Phe}–EF-Tu–GTP and Lys-tRNA^{Lys}–EF-Tu–GTP) were prepared with the GTP-regenerating buffer as described by Fei *et al.*[25]. The reactions were assembled in sequential order: the 70S IC was first incubated for 1 min with either Polymix buffer with 3.5 mM $Mg(OAc)_2$ containing 0.5 mM Mg-ATP or with EttA-EQ_2 (6 μM) with Mg-ATP (0.5 mM), then incubated for 1 min with ternary complex, and then incubated for the indicated reaction time with EF-G. After hydrolysis of the product with 0.2 M of KOH, reaction products were separated by electrophoretic thin layer chromatography (eTLC) as described by Youngman *et al.*[52] and quantified by phosphorimaging. Specifically, 0.5 μl of each sample was spotted onto TLC-cellulose (EMD Chemicals) plates, dried and separated by electrophoresis in pyridine acetate buffer, pH 2.8 (20% glacial acetic acid and 0.06% pyridine), at 1,200 V for 20 min.

Cryo-EM sample preparation. The cryo-EM sample was prepared in the same way as in the peptide formation assay, with minor modifications. 70S IC complex was assembled as described above, but the [^{35}S]fMet-tRNA^{fMet} was replaced by the same amount of fMet-tRNA^{fMet}. The 70S IC complex was incubated with EttA-EQ_2 (6 μM) at 37 °C for 1 min, then with Phe-tRNA^{Phe}–EF-Tu–GTP ternary complex (0.67 μM) at 37 °C for 1 min. The mixture was then kept at room temperature (~25 °C) and diluted ten-fold with Polymix buffer containing 3.5 mM Mg-ATP right before (within 1 min) preparation of the cryo-EM grids, as described by Grassucci *et al.*[23]. Specifically, the diluted sample was applied on a hydrophilic Quantifoil (Jena, Germany) R2/4 300 mesh Cu EM grid, incubated for 30 s at 4 °C and 100% relative humidity, then plunge-frozen in liquid ethane (approximately −183 °C) with a Vitrobot Mark IV (FEI, Hillsboro, Oregon).

Cryo-EM data collection, single-particle reconstruction and classification. *Cryo-EM data collection.* The cryo-EM data were collected, as previously described[23], in low-dose mode on an FEI (Hillsboro, Oregon) Tecnai F20 TEM at 200-kV extraction voltage and ~80,000× magnification with the automatic image collection program Leginon[53]. Micrographs were recorded on a Gatan (Warrendale, PA) UltraScan 4000 CCD camera binned by 2× with effective CCD magnification of 110,637× and pixel size of 2.71 Å on the object scale.

Single-particle reconstruction. For reference-based single-particle reconstruction with SPIDER[24,54], a total of 2,390 CCD micrographs were selected, which had visible particles and perfectly round Thon rings. These micrographs were separated evenly into 40 defocus groups with total defocus range of −3.5 μm to −1.2 μm. With a cryo-EM map of the empty ribosome[27], low-pass-filtered to 15-Å resolution, used as reference, 108,691 ribosome particles were chosen via automatic particle picking[55] and subsequent visual verification. The 3D reconstruction from this total data set was iteratively refined with SPIDER[54] to 8.2-Å resolution (FSC = 0.5 criterion) and subjected to amplitude correction[56]. The cryo-EM map of the total data set revealed a 70S ribosome containing densities at the A and P sites that were attributable to A- and P-site tRNAs, as well as additional density at the E site that was not attributable to an E-site tRNA (visually similar to **Fig. 1**).

Computational classification. The cryo-EM map of the total data set revealed weaker densities for the A- and P-site tRNAs relative to 23S rRNA of the 50S subunit, thus indicating heterogeneity in the total data set, i.e., ribosome particles being in different conformations and/or containing different components. Therefore, we used RELION[57,58] in a stepwise hierarchical classification (**Supplementary Fig. 3a**, with methods described in the **Supplementary Note**).

Resolution measurement with gold-standard FSC[59]. For each data set, the RELION 3D autorefine program was used to independently refine, from randomly split half data sets, the two unfiltered half volumes, with resolution reported by the gold-standard criterion. To eliminate peripheral noise and recalculate the resolution, we also used SPIDER commands to multiply these two unfiltered half volumes with a soft Gaussian mask having 0.5 fall-off at 3 pixels (8.1 Å) outside the ribosomal complex, and calculated the Fourier shell correlation (FSC) between the two masked half volumes. The FSC versus spatial frequency curves were plotted (**Supplementary Fig. 3b**). The resolution of each map was then determined with the FSC = 0.143 criterion. The gold-standard resolutions, before (i.e., reported by RELION 3D auto-refine) and after application of the soft Gaussian mask, for each 70S ribosome class are: class I, 8.5 Å (7.5 Å); class II, 10.1 Å (9.1 Å); and class III, 8.7 Å (7.7 Å).

Molecular dynamics flexible fitting (MDFF) of EttA-bound 70S ribosome complex. *Modeling of ATP-bound EttA monomeric structure* (**Fig. 4**). First, we

doi:10.1038/nsmb.2741

generated a monomeric apo-EttA structure model by combining residues 1–277 of one protomer and residues 278–542 of the other protomer in the apo-EttA$_2$ crystallographic structure[4]. Second, we matched this apo-EttA model to the ATP-bound head-to-tail homodimer crystallographic structure of cystic fibrosis transmembrane conductance regulator (CFTR) nucleotide binding domain 1 (NBD1) (PDB 2PZE[30]), an ABC transporter homologous to EttA[4], by separately aligning the core and the helical subdomains, as previously described[60], to account for the subdomain rotation in ABC domains[31]. Third, we complemented the secondary structures of missing links in the aligned EttA model with Protein Homology/analogY Recognition Engine (Phyre 2) server[61] search hits. Specifically, the missing residues of the EttA arm (residues 132–140), inter–ABC-domain linker helices (residues 243–279, which we call PtIM) and C-terminal helix (residues 543–555) were modeled on the basis of parts of PDB 1UO0, 1ABZ and 2BBM, respectively. Cross-correlation coefficient (CCC) to the EttA-EQ$_2$ isolated density map in class I was calculated in UCSF Chimera[62] with simulated maps from atomic structures filtered to 7-Å resolution. The CCC value was 0.91 for the ATP-bound EttA monomer model versus 0.83 for the nucleotide-free EttA monomer model, thus indicating that the ribosome-bound EttA-EQ$_2$ is in the ATP-bound conformation.

MDFF of EttA-bound 70S ribosome complex. The initial system for MDFF[29] was prepared with VMD[63] and consisted of the *E. coli* 70S ribosome (PDB 3R8O and 3R8T[64]), an mRNA coding for Met-Phe with 12 nucleotides of 5′ untranslated region (a combination of PDB 3R8O[64] and 3FIH[65]), P-site tRNA^{fMet} and A-site tRNA^{Phe} (PDB 2WDG[37], with amino acids on tRNAs computationally removed), and ATP-bound monomeric EttA structure model.

Because of the different conformation of the L1 stalk in our reconstruction compared to the *E. coli* 70S X-ray structure in the initial system, a short *in vacuo* MDFF run was first performed on the initial system lacking EttA structure model, to bring the L1 stalk to the widely open conformation observed in our cryo-EM reconstruction. For this *in vacuo* run, the density map used was the class I map with the EttA density computationally removed with SPIDER. This initial system lacking EttA was first rigid-body-fitted into the class I map using the FIT IN MAP module implemented in Chimera[62]. Starting from this initial fit, the intermolecular steric clashes were fixed by manual adjustment of some of the side chains of proteins and nitrogenous bases of RNAs with PyMOL (http://www.pymol.org/). The system was minimized for 1,000 steps in NAMD[66] and subsequently by MDFF[29], which applies a potential to the systems on the basis of the cryo-EM density map. The run was stopped after 300 ps, when the L1 stalk stabilized in the open conformation. We call the obtained model open-L1 70S, comprising the *E. coli* 70S ribosome, A-site tRNA^{Phe}, P-site tRNA^{fMet} and an mRNA.

Next, the open-L1 70S and ATP-bound EttA structure models were rigid-body-fitted into the class I cryo-EM map, with the EttA model binding to the E site, using the FIT IN MAP module in Chimera. The intermolecular steric clashes were fixed manually with PyMOL. The whole system was then minimized for 1,000 steps in NAMD and subsequent *in vacuo* MDFF in NAMD for 300 ps to relax the system in the presence of EttA. In order to have a better representation of the inter- and intramolecular interaction, the whole system was then embedded in a solvent box of TIP3P water molecules with an extra 12-Å padding in each direction, and negative charges of the ribosome complex were neutralized with potassium ions with an excess amount of ~0.2 M KCl. The whole system was then minimized for 3,000 steps in NAMD and subsequently by MDFF. The in-solvent MDFF was equilibrated over 350 ps by application of harmonic positional constraints staring at 5.0 kcal/(mol×Å) and decreasing it progressively till 0.1 kcal/(mol×Å) upon starting the trajectories production phase with no harmonic constraints. The run was stopped at 700 ps of simulation time, after the whole system converged as estimated by the r.m.s. deviation and cross-correlation coefficient (CCC) values (**Supplementary Fig. 4**). All the simulated systems were prepared with CHARMM[67,68] force-field parameters (combining CHARMM all-hydrogen topology file for CHARMM22 proteins and CHARMM27 lipids).

Solvent-accessible surface area was measured with PyMOL. The density map of the X-ray structure was converted with UCSF Chimera[62]. Figures were generated with UCSF Chimera[62] and PyMOL.

E-site binding competition assay. *Deacylated [^{32}P]tRNA^{Phe}synthesis*[69,70]. 34 μM of tRNA^{Phe} (Sigma-Aldrich) was incubated with 50 mM of glycine, pH 9, 10 mM $MgCl_2$, 360 Ci/mmol [α-^{32}P]ATP (PerkinElmer), 0.05 mM sodium pyrophosphate and 0.03 mg/ml of nucleotidyl transferase. The reaction was incubated for 5 min at 37 °C. Radioactively labeled tRNA was purified by phenol/chloroform extraction and subsequent ethanol precipitation, resuspended in milliQ water and filtered through a P6 column (Bio-Rad) pre-equilibrated with milliQ water in order to remove unincorporated radioactivity.

E-site binding filter assay. The assay was based on the original assay of Grajevskaja *et al.*[26] used in the discovery of the E site. The 70S ribosomes used for the assay were prepared as for the minimal *in vitro*–purified translation assay[4]. 70S ribosomes (0.2 μM) were incubated in the presence of increasing concentrations of EttA-EQ$_2$ (0, 0.2, 0.4, 0.8, 1.0, and 1.2 μM) and deacylated [^{32}P]tRNA^{Phe} (0.4 μM) for 2 min at 4 °C in 0.1 mM ATP, 10 mM $Mg(OAc)_2$, 100 mM NH_4Cl, 20 mM Tris-HCl, pH 7.4, in a 20 μl reaction. 5 μl of each reaction was spotted on a nitrocellulose filter (25 mm, 0.45 μm, nitrocellulose, disc filters, Millipore) installed on a sampling manifold (Millipore) under constant vacuum. After three washes with 2 ml of 20 mM $Mg(OAc)_2$, 100 mM NH_4Cl, 1 mM EDTA and 20 mM Tris-HCl, pH 7.4, the filters were immersed in scintillation liquid (Ultima Gold, PerkinElmer) and counted on a scintillation counter (Beckman LS6500). 5 μl of each reaction was also counted without being spotted on a nitrocellulose filter or washed, to give the total radioactivity in each reaction. The ratios of radioactivity retained on the filter versus total were calculated and adjusted to the moles of ribosome in each reaction.

Curve fitting and analysis. EttA-EQ$_2$ was used to drive displacement of deacylated tRNA from the ribosomal E site in the absence of A-site tRNA (**Fig. 2**). The binding affinity of this mutant variant of EttA for the ribosome in the presence of Mg-ATP was inferred from the resulting data on the basis of the following competitive-binding model:

$$\text{ribosome}-\text{EttA} \leftrightarrow \text{EttA}_{\text{free}} + \text{ribosome}_{\text{free}} + \text{tRNA}_{\text{free}} \leftrightarrow \text{ribosome}-\text{tRNA}$$

In this chemical equation, the species in the middle represent the free forms of the interaction partners, whereas those on the left and right represent the two competing E-site complexes. The dissociation constants for the competing complexes are given by the following expressions:

$$K_{\text{d-EttA}} = [\text{EttA}_{\text{free}}][\text{ribosome}_{\text{free}}]/[\text{ribosome}-\text{EttA}]$$
$$K_{\text{d-tRNA}} = [\text{tRNA}_{\text{free}}][\text{ribosome}_{\text{free}}]/[\text{ribosome}-\text{tRNA}]$$

This binding model yields the following equation describing the fractional concentration of tRNA remaining bound to the ribosome (Y) in the presence of a given total concentration of EttA ([EttA$_{total}$]) compared to that bound before initiation of the titration ([ribosome–tRNA]$_0$)

$$Y([\text{EttA}_{\text{total}}]) = [\text{ribosome}-\text{tRNA}]([\text{EttA}_{\text{total}}])/[\text{ribosome}-\text{tRNA}]_0 =$$
$$(1 + ([\text{tRNA}_{\text{total}}]/K_{\text{d-tRNA}}))/(1 + ([\text{tRNA}_{\text{total}}]/K_{\text{d-tRNA}}) + ([\text{EttA}_{\text{total}}]/K_{\text{d-EttA}}))$$

The parameter [tRNA$_{total}$] represents the total concentration of the deacylated tRNA included in the assay (400 nM). The value of $K_{d\text{-tRNA}}$ under assay conditions was determined to be 111 nM, on the basis of quantification of the radioactive tRNA bound to ribosomes compared to the total amount of radioactive tRNA before addition of any EttA, which was used to calculate the free and bound concentrations of tRNA and ribosome. The last equation above was used to fit the data in **Figure 2** in the main text after appropriate factors were included to scale it to the experimental data

$$R([\text{EttA}_{\text{total}}]) = B + \Delta \times Y([\text{EttA}_{\text{total}}])$$

In this equation, R([EttA$_{total}$]) represents the measured fraction of ribosomes with tRNA bound in the presence of a given total concentration of EttA compared to that bound in the absence of EttA, B is the background level and Δ is a linear scale factor normalizing for the fraction of ribosomes bound in the absence of EttA. Curve-fitting was performed with the algorithm of Marquardt and Levenberg as implemented in PRISM (version 5.0c for Mac OS X, http://www.graphpad.com/), constraining the parameter B to be greater than or equal to zero. The best-fit values ± s.e. are: $K_{d\text{-EttA}} = 47 \pm 12$ nM, $B = 0$, and $\Delta = 0.72 \pm 0.05$.

51. Fei, J., Richard, A.C., Bronson, J.E. & Gonzalez, R.L. Transfer RNA-mediated regulation of ribosome dynamics during protein synthesis. *Nat. Struct. Mol. Biol.* **18**, 1043–1051 (2011).

52. Youngman, E.M., Brunelle, J.L., Kochaniak, A.B. & Green, R. The active site of the ribosome is composed of two layers of conserved nucleotides with distinct roles in peptide bond formation and peptide release. *Cell* **117**, 589–599 (2004).
53. Suloway, C. *et al.* Automated molecular microscopy: the new Leginon system. *J. Struct. Biol.* **151**, 41–60 (2005).
54. Shaikh, T.R. *et al.* SPIDER image processing for single-particle reconstruction of biological macromolecules from electron micrographs. *Nat. Protoc.* **3**, 1941–1974 (2008).
55. Rath, B.K. & Frank, J. Fast automatic particle picking from cryo-electron micrographs using a locally normalized cross-correlation function: a case study. *J. Struct. Biol.* **145**, 84–90 (2004).
56. Gabashvili, I.S. *et al.* Solution structure of the *E. coli* 70S ribosome at 11.5 Å resolution. *Cell* **100**, 537–549 (2000).
57. Scheres, S.H.W. A Bayesian view on cryo-EM structure determination. *J. Mol. Biol.* **415**, 406–418 (2012).
58. Scheres, S.H.W. RELION: implementation of a Bayesian approach to cryo-EM structure determination. *J. Struct. Biol.* **180**, 519–530 (2012).
59. Scheres, S.H. & Chen, S. Prevention of overfitting in cryo-EM structure determination. *Nat. Methods* **9**, 853–854 (2012).
60. Lewis, H.A. *et al.* Structure and dynamics of NBD1 from CFTR characterized using crystallography and hydrogen/deuterium exchange mass spectrometry. *J. Mol. Biol.* **396**, 406–430 (2010).
61. Kelley, L.A. & Sternberg, M.J.E. Protein structure prediction on the Web: a case study using the Phyre server. *Nat. Protoc.* **4**, 363–371 (2009).
62. Pettersen, E.F. *et al.* UCSF Chimera: a visualization system for exploratory research and analysis. *J. Comput. Chem.* **25**, 1605–1612 (2004).
63. Humphrey, W., Dalke, A. & Schulten, K. VMD: visual molecular dynamics. *J. Mol. Graph.* **14**, 33–38 (1996).
64. Dunkle, J.A. *et al.* Structures of the bacterial ribosome in classical and hybrid states of tRNA binding. *Science* **332**, 981–984 (2011).
65. Villa, E. *et al.* Ribosome-induced changes in elongation factor Tu conformation control GTP hydrolysis. *Proc. Natl. Acad. Sci. USA* **106**, 1063–1068 (2009).
66. Phillips, J.C. *et al.* Scalable molecular dynamics with NAMD. *J. Comput. Chem.* **26**, 1781–1802 (2005).
67. Brooks, B.R. *et al.* CHARMM: A program for macromolecular energy, minimization, and dynamics calculations. *J. Comput. Chem.* **4**, 187–217 (1983).
68. MacKerell, A.D. *et al.* in *The Encyclopedia of Computational Chemistry*, Vol. 1 (eds. Schleyer, P.v.R. *et al.*) 271–277 (John Wiley & Sons, 1998).
69. Ledoux, S. & Uhlenbeck, O.C. [3′-32P]-labeling tRNA with nucleotidyltransferase for assaying aminoacylation and peptide bond formation. *Methods* **44**, 74–80 (2008).
70. Wolfson, A.D. & Uhlenbeck, O.C. Modulation of $tRNA^{Ala}$ identity by inorganic pyrophosphatase. *Proc. Natl. Acad. Sci. USA* **99**, 5965–5970 (2002).

doi:10.1038/nsmb.2741